2015

Ultra-weak intrinsic FP cavity array for distributed sensing

Zhen Chen
University of Rhode Island

Lei Yuan

See next page for additional authors

Citation/Publisher Attribution
Zhen Chen, Lei Yuan, Gerald Hefferman, and Tao Wei, "Ultraweak intrinsic Fabry–Perot cavity array for distributed sensing," Opt. Lett. **40**, 320-323 (2015).
Available: http://dx.doi.org/10.1364/OL.40.000320

Ultra-weak intrinsic FP cavity array for distributed sensing

Zhen Chen,[1] Lei Yuan,[2] Gerald Hefferman,[1,3] and Tao Wei[1,*]

[1]*Department of Electrical, Computer and Biomedical Engineering, University of Rhode Island, Kingston, RI, 02881, USA*
[2]*Department of Electrical and Computer Engineering, Clemson University, Clemson, SC, 29634, USA*
[3]*Warren Alpert Medical School of Brown University, Providence, RI, 02903, USA*
**Corresponding author: wei@ele.uri.edu*

Received Month Oct, 2014; revised Month X, XXXX; accepted Month X, XXXX;
posted Month X, XXXX (Doc. ID XXXXX); published Month X, XXXX

This letter reports an ultra-weak intrinsic Fabry–Pérot interferometer (IFPI) array fabricated by femtosecond (fs) laser for distributed sensing applications. Ultra-low reflectors (<–60 dB) were obtained. IFPIs with different physical lengths showed identical temperature sensitivity (–1.5 GHz/°C). A distributed temperature sensing test was conducted. No crosstalk between IFPI elements in the array was observed, implying the device's utility as a distributed sensing system. The possibility of using smaller bandwidths for sensor interrogation was experimentally proven. A small-scale temperature distribution test was conducted on a continuously cascaded ultra-weak IFPI array, demonstrating its high spatial resolution. The temperature detection limit of this system was measured to be less than 0.0667°C.
OCIS Codes: (060.2370) Fiber optics sensors.
http://dx.doi.org/10.1364/OL.99.099999

Distributed optical fiber sensing technology is a thriving branch of sensing technology, due in large part to its ability to surmount many limitations of traditional single-point sensor, enabling a single system to simultaneously span a large number of equivalently individual sensors [1]. These unique advantages have been successfully demonstrated in many application areas, including oil drilling, structural health monitoring, and perimeter security [2]. The recent development of distributed optical fiber sensors with high spatial resolution has expanded this utility considerably, making it an attractive addition to many emerging applications, such as wearable devices, robotics, and surgical instrument [3, 4].

The use of Rayleigh scattering as a sensing method has shown particular promise in distributed sensing with high spatial resolution [5]. The unique Rayleigh backscattering profile of a section of optical fiber can be extracted via swept-frequency interferometry, revealing the profile of ambient temperature and strain change along the length of the fiber. By sweeping over a broad optical bandwidth, this technology can resolve minute changes in Rayleigh backscattering profile with mm-level spatial resolution. However, this modality requires the interrogating laser to sweep over a broad wavelength range with high coherence length, limiting the update rate of the measurement system. Additionally, broadband, highly coherent, and single longitudinal mode swept lasers come at considerable cost.

Weak fiber Bragg grating (FBG) arrays represent another technology breakthrough in this area [6]. A large number of low reflection FBGs with same nominal resonant wavelength are fabricated along an optical fiber in a discrete fashion, known as weak FBG sensor network, or in a continuous fashion, known as long-length FBG [7]. The sensing mechanism of an individual weak FBG is the same conventional FBG; however, in contrast to the wavelength domain multiplexing (WDM) technology used for traditional FBGs, a weak FBG array is multiplexed in the spatial domain. The low reflectivity of each individual FBG element ensures minimal crosstalk among FBGs in an array. Researchers have demonstrated several probing technologies to interrogate weak FBG arrays, including combined wavelength-time-domain reflectometry, optical frequency domain reflectometry (OFDR), and synthesis of optical coherence function (SOCF) method [6, 7]. The responses of thousands of individual weak FBGs in a single array can be measured simultaneously. In comparison with the Rayleigh scattering approach, weak FBGs require a significantly smaller wavelength range for sensor interrogation, leading to a higher update rate. Currently, a weak FBG array is fabricated during the fiber drawing process and features a reflectivity of ~ –33 dB [8].

There exists another highly sensitive, miniature-scale, and low reflection device in the optical fiber sensor family – intrinsic Fabry–Pérot interferometer (IFPI). This technology uses a pair of small reflectors introduced in an optical fiber, forming a cavity that creates interferogram in the wavelength domain. Ambient physical changes are detected through shifts of the resulting interferogram. Traditionally, the reflectors of IFPIs are fabricated via splicing together different optical fibers of differing refractive indices or via exposing a fiber to intense UV light [9]. Recent technology advances have led to increased popularity in the use of femtosecond (fs) lasers in fabricating fiber optic devices [10, 11]. Weak reflectors with a reflectivity of ~ –45 dB were achieved to form IFPIs with this fabrication method [12]. An FFT-based method was used to multiplex 3 IFPIs of differing cavity lengths. Very recently, Huang et al. successfully demonstrated an optical carrier based microwave interferometry method to simultaneously interrogate identical and cascaded IPFIs with a length of 12 cm along an optical fiber [13]. However, the low microwave frequency bandwidth limits its spatial resolution.

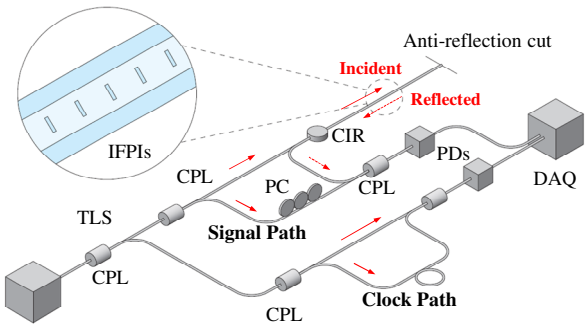

Fig. 1. Schematic of the interrogation system for IFPI arrays

This letter reports a fiber-inline ultra-weak (<−60 dB) IFPI array fabricated using fs laser for distributed sensing with high spatial resolution. Interrogation approach, fabrication parameters, sensitivity, operation bandwidth, and distributed sensing ability of the proposed IFPI array were experimentally investigated in this letter.

The Schematic of the interrogation system, based on OFDR, is drawn in Figure 1. Light from a tunable laser source (TLS) is split into two paths – "clock" and "signal". "Clock" is an interferometer used to calibrate the non-linear sweep effect of the TLS by providing a corrected time base for a data acquisition card (DAQ) during frequency sweep. A comparator circuit was designed to receive "clock" signal to trigger the DAQ card to sample "signal" data. Due to the non-linear sweep effect, the sampling rate is not a constant, and the maximum rate is below 1 MSa/sec. Light in the "signal" section is split between the reference and measurement arms of an interferometer via a 50/50 coupler (CPL); in the measurement path, an optical circulator (CIR) further splits the light to interrogate the low-reflection IFPI array and returns the reflected light. A polarization controller (PC) is used to tune the state of polarization in the system. Another 50/50 CPL then recombines the measurement and reference fields. In this setup, the TLS sweeps from 1535 to 1565 nm at a speed of 16 nm/s, covering a total bandwidth of 3.7 THz. The interrogation is operated in real-time with single measurement duration of around 3 sec, which includes 2 sec for laser scanning, and 1 sec for the DAQ to transfer data to a computer and its calculation time in the computer. Thus, the AC-coupled voltage received by the DAQ is written as:

$$v_{total} = 2\,\eta\,r\,I_{ref}\,\sum_{n=1}^{N-1} cos\left[\beta\left(z_{ref} - z_n\right)\right] \quad (1)$$

where η is the light-to-voltage conversion coefficient of the photodetector, r is the reflection coefficient of the reflector of the IFPI, I_{ref} is the light intensity of the reference arm, N is the number of reflectors along the optical fiber, β is the propagation constant, z_{ref} is the length of reference fiber, and z_n represents the position of n^{th} reflector. The intensity of the reflected light as a function of position can be readily obtained via a Fourier transform. It is worth noting that Rayleigh backscatter in this system is considered as noise floor in this study. Two neighboring reflectors form an IFPI, which can be time-gated and extracted via a digital bandpass filter.

A Ti: Sapphire fs laser (Coherent, Inc.) micromachining system was used to fabricate ultra-weak reflectors. The

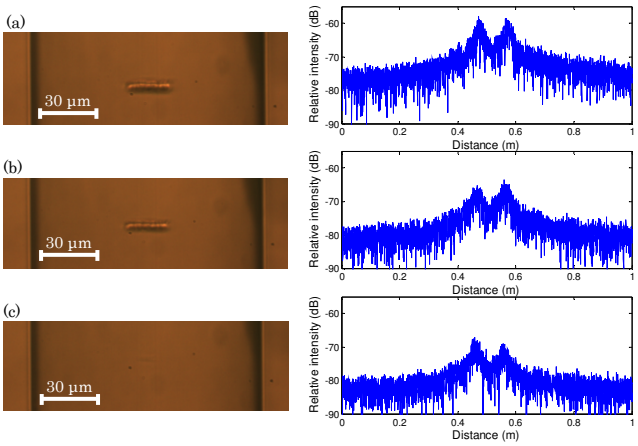

Fig. 2. Microscopic image (top view) of single weak reflector created by fs laser, and the corresponding reflection distribution in spatial domain of three 1 cm IFPI cavities fabricated with differing laser power: (a) 0.14, (b) 0.12, and (c) 0.1 W.

central wavelength, pulse width, repetition rate, and maximum power of the laser are 800 nm, 200 fs, 250 kHz, and 1 W, respectively. The actual power used for fabrication is controlled by adjusting a half-wave plate, a polarizer, and several neutral density (ND) filters. The laser was switched on or off by electrically gating the internal clock. A single-mode optical fiber (Corning, SMF-28e) with the core and cladding diameters of 8.2 and 125 μm, respectively, was used for these experimental trials. After mechanically stripping its buffer, the fiber was cleaned using acetone and clamped onto two bare fiber holders, which were immersed in distilled water during fabrication. The fiber assembly was mounted on a computer-controlled three-axis translation stage with a resolution of 0.1 μm (Newport, Inc.). The fs laser beam was focused inside the optical fiber through a water immersion objective lens (Olympus UMPlanFL 20x) with a numerical aperture (NA) of 0.4. The velocities of the stages were set at 50 μm/s during fabrication. A cuboid region (10×2×10 μm) was inscribed in the center of the fiber from bottom up to cover the whole cross-section of the fiber core. The center of the inscribed region was aligned with the center of the fiber core. Figure 2 shows both the microscopic images and reflection distribution of three IFPIs fabricated with different fs laser powers (0.14, 0.12, and 0.1 W). The reflection values measured using the interrogation system were referenced to an angled polished connector (APC), which was previously measured using off-the-shelf precision instruments. The reflectivity of the weak reflectors decreased as fabrication power was reduced. A reflectivity of around −70 dB was achieved with laser beam at 0.1 W. In this study, 0.14 W was chosen as the fs laser power used for IFPI fabrication.

The sensing mechanism of an IFPI is based on tracking the phase shift of the interferogram in response to ambient change. To extract the phase shift information from the signal received from an individual IFPI, the reflection signal in frequency-domain is squared and filtered using a low-pass filter to obtain the interference signal (S):

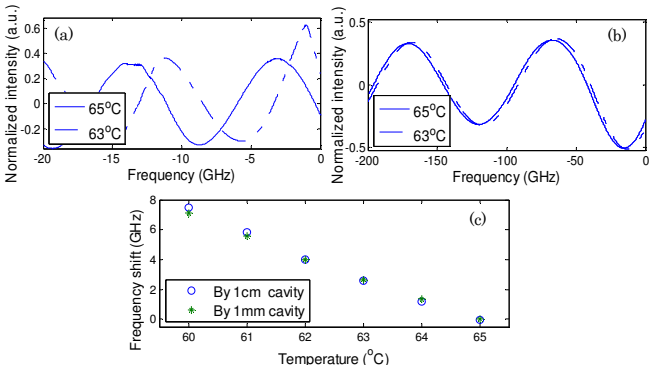

Fig. 3. Temperature responses of IFPIs of differing lengths: (a) interferogram of a 1 cm IFPI at 63˚C and 65˚C; (b) interferogram of a 1 mm IFPI at 63˚C and 65˚C; and (c) frequency shifts as a function of temperature for both 1 cm and 1 mm IFPIs.

$$S = 4\eta^2 r^2 I_{ref}^2 \cos\left(\frac{4\pi\, n_{eff}\, Lf}{c}\right) \qquad (2)$$

where L is the physical cavity length of IFPI, n_{eff} is the effective refractive index of the fiber, f is the frequency of the laser, and c is the velocity of light in vacuum. Additionally, $n_{eff}L$ is considered the optical length of the IFPI cavity. From Equation (2), as optical length increases, the period of the cosine function with respect to laser frequency decreases. As a result, at laser frequencies (~193 THz), the interference signal shifts to smaller frequencies, proportionally.

To investigate ultra-weak IFPI sensors, two IFPIs with lengths of 1 cm and 1 mm, respectively, were fabricated. The temperature response of both IFPIs was measured using a temperature-controlled water bath. Figures 3(a) and 3(b) plot the measured interferogram of both IFPIs at 63˚C and 65˚C, where the x-axis is the frequency offset from the start of frequency sweep. As temperature increases, the optical length of both IFPIs increases, leading to an interferogram shift towards lower frequency. The frequency shift of interferogram is determined via tracking its zero-crossing position. This technique is justified by the fact that steepest slope of a sinusoidal function occurs at its zero-crossing position. Figure 3(c) depicts the frequency shift of the interferogram as a function of temperature for both IFPIs. The temperature sensitivity of both 1 cm and 1 mm IFPIs was measured to be around −1.5 GHz/ ˚C, agreeing well with the theory value [12]. Comparing the two IFPIs, the interference period with respect to frequency for the 1 cm IFPI is 1/10 of the 1 mm IFPI. As a result, the 1 cm IFPI is more subject to 2π ambiguity problem, limiting its measurement dynamic range. However, the slope of the 1 cm IFPI at zero-crossing position is ten times higher than that of the 1 mm IFPI, leading to a much higher accuracy. As a result, an IFPI with a longer length is suitable for precisely measuring smaller physical changes.

To demonstrate the distributed sensing capability of ultra-weak IFPIs, three identical 1 cm IFPIs were fabricated and spliced along a single fiber line. Figure 4(a) depicts the reflection distributions of the 3 ultra-weak-IFPIs, which were spaced approximately 1.5 m apart. The 2nd IFPI (middle) was immersed in a temperature-controlled water bath, while the 1st and 3rd IFPIs were left

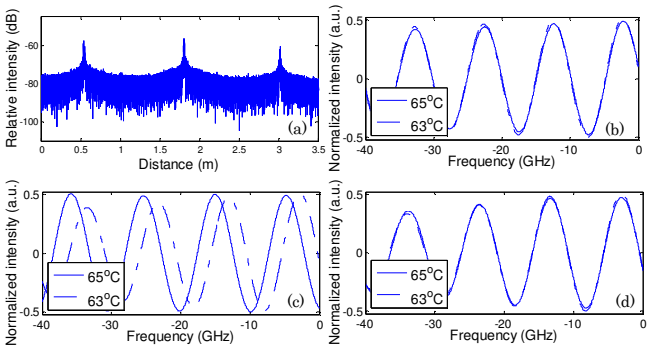

Fig. 4. Demonstration of ultra-weak IFPIs for distributed sensing, where only the 2nd IFPI is subject to temperature change: (a) reflection distributions of 3 IFPIs; (b) interferogram of 1st IFPI when ambient temperature of 2nd IFPI is varied; (c) interferogram of 2st IFPI at 63˚C and 65˚C; (d) interferogram of 3rd IFPI when temperature of 2nd IFPI is varied.

unchanged at ambient temperature. The water bath was heated to 65°C and cooled down to 63°C. Three bandpass filters were used to gate the 3 IFPIs in time-domain and extract the interferograms of all 3 IFPIs in frequency-domain, shown in Figures 4(b)-(d). As expected, the interferogram of the 2nd IFPI shifted to higher frequencies as temperature decreased. Concurrently, the 1st and 3rd interferogram remained unchanged. No crosstalk was observed between IFPIs in this experiment, indicating that this technology holds considerable potential for distributed sensing applications.

A key advantage of an IFPI array over the Rayleigh scattering method is that an IFPI does not require a large bandwidth to resolve small changes with high spatial resolution. To demonstrate this feature, a 1 cm IFPI was experimentally tested using different laser sweeping bandwidths. Figures 5(a)-(c) depict the interferograms of the IFPI at 63˚C and 65˚C with 3 laser sweeping bandwidths. It can be observed that the interferograms generated using these different interrogation bandwidths are similar. The identical temperature response with different sweeping bandwidths, shown in Figure 5(d), further confirms IFPI's capability to operate within relatively narrow bandwidths.

To investigate the spatial resolution of the proposed

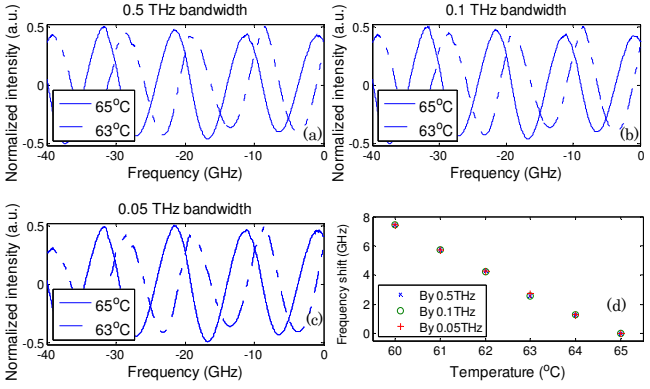

Fig. 5. Temperature response of a 1 cm IFPI interrogated using different laser sweeping ranges: (a)-(c) interferogram of the IFPI (d) temperature response with 3 interrogation bandwidths.

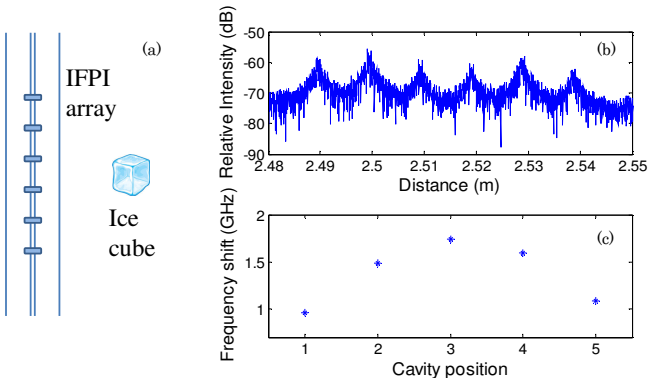

Fig. 6. Experimental study of continuously cascaded ultra-weak IFPIs: (a) test setup; (b) reflection distribution of 5 IFPIs; (c) frequency distribution measured using IFPI array.

technology, an IFPI array was fabricated along the fiber in a continuous fashion with identical individual cavity length to be 1 cm. The reflection distribution of this array is depicted in Figure 6(b), which spans 5 cm. The reflectivity of reflectors in this array is around −60 dB. The interferograms of all 5 IFPIs were first measured as a reference. Then, a cube of ice was placed ~1 cm away from the center of the IFPI array as sketched in in Figure 6(a). The interferograms were again taken, and the frequency shifts as a function of IFPI location plotted in Figure 6(c). A Gaussian-like temperature distribution was observed, in which the center IFPI experienced a temperature around 1˚C lower than IFPIs at either edge as expected. This experiment proves that continuously cascaded IFPIs can be used for distributed sensing. The spatial resolution is the cavity length of the individual IFPIs, i.e., 1 cm in this test.

To evaluate system-level accuracy, a stability test was conducted by fixing the ambient condition of a 1 cm IFPI. 100 groups of interferogram were generated using this device. The frequency shift of each interferogram relative to its initial status was calculated. The standard deviation of the frequency shift is less than 100 MHz, determining the system's detection limit. Given the experimentally measured sensitivity of −1.5 GHz/˚C, its temperature detection limit is calculated to be less than 0.067 ˚C.

Previous studies of weak FBG sensors suggest that the multiplexing capacity is mainly limited by two types of crosstalk [6]. The first is spectral shadowing – spectral distortion of the downstream devices caused by the insertion loss of the upstream devices; the second is multiple-reflection crosstalk, or the spectral distortion induced by false signals, which undergo multiple reflections between upstream devices, and experiences the same time delay as the real signal. Both types of crosstalk are exponentially proportional to the reflectivity of the device. Ideally, the reflectivity of an IFPI is calculated by doubling the reflectivity of single reflector. The smallest reflector achieved in our lab was −72 dB, converted to a −69 dB IFPI, which is more than 30 dB smaller than the current ultra-weak FBGs. A theoretic model was applied to estimate the multiplexing capacity of the proposed ultra-weak IFPI sensor array [6]. Spectral shadowing effect was simulated in a sensor array of 100,000 IFPIs. In this model, the frequency shifts of all upstream sensors can maximally contribute an unwanted spectral shift of 63.64 MHz to the last IFPI, converted to a reasonable temperature measurement uncertainty of 0.042˚C. In addition, when multiple-reflection crosstalk is considered as the only noise source, a total multiplexing number of 1 million maintains a signal-to-noise ratio (SNR) of 20 dB, indicating its negligible influence. To summarize, 100,000 is approximated as the system's multiplexing capacity. In practice, this number will decrease due to the coherence length limit, total length of fiber, detector quality, and unwanted extra loss along the fiber. Nevertheless, the proposed ultra-weak IFPI array technology holds considerable potential to increase the multiplexing capacity by orders of magnitude beyond current methods.

To conclude, we reported an ultra-weak IFPI array fabricated by fs laser for distributed sensing applications. Reflectivity of weak reflectors decreases as the fs laser power is reduced. IFPI cavities with different physical lengths (1 cm and 1 mm) showed identical temperature sensitivity (−1.5 GHz/˚C). A distributed temperature sensing test was conducted and no crosstalk between IFPI elements observed, implying utility as a distributed sensing system. The system was experimentally proven to be capable of operating within a small bandwidth. A small-scale temperature distribution test was conducted on a continuously cascaded ultra-weak IFPI array, demonstrating its high spatial resolution. The temperature detection limit of this system was measured to be less than 0.0667 ˚C.

This research was sponsored in part by NSF CCF-1439011.

References

1. J. Huang, L. Hua, X. Lan, T. Wei, and H. Xiao, Optics Express **21**, 18152-18159 (2013).
2. X. Bao, and L. Chen, Sensors **12**, 8601-8639 (2012).
3. L. Thévenaz, S. Foaleng-Mafang, K.-Y. Song, S. Chin, J.-C. Beugnot, N. Primerov, and M. Tur, in (EWOFS'10) Fourth European Workshop on Optical Fibre Sensors, pp. 765309-765309-765307.
4. G. M. Prisco, Patent US7772541, 2012.
5. M. Froggatt, and J. Moore, Applied Optics **37**, 1735-1740 (1998).
6. Y. Wang, J. Gong, B. Dong, D. Y. Wang, T. J. Shillig, and A. Wang, Lightwave Technology, Journal of **30**, 2751-2756 (2012).
7. K. Hotate, and K. Kajiwara, Optics Express **16**, 7881-7887 (2008).
8. D. Johnson, Laser Focus World **48**, 53 (2012).
9. F. Shen, W. Peng, K. L. Cooper, G. Pickrell, and A. Wang, in Optics East, SPIE, 2004, pp. 47-56.
10. L. Yuan, J. Huang, X. Lan, H. Wang, L. Jiang, and H. Xiao, Optics Letters **39**, 2358-2361 (2014).
11. Y. Zhang, L. Yuan, X. Lan, A. Kaur, J. Huang, and H. Xiao, Optics Letters **38**, 4609-4612 (2013).
12. W. Wang, D. Ding, N. Chen, F. Pang, and T. Wang, Sensors Journal, IEEE **12**, 2875-2880 (2012).
13. J. Huang, X. Lan, M. Luo, and H. Xiao, Optics Express **22**, 18757-18769 (2014).

Full Reference List

1. J. Huang, L. Hua, X. Lan, T. Wei, and H. Xiao, "Microwave assisted reconstruction of optical interferograms for distributed fiber optic sensing," Optics Express **21**, 18152-18159 (2013).
2. X. Bao, and L. Chen, "Recent progress in distributed fiber optic sensors," Sensors **12**, 8601-8639 (2012).
3. L. Thévenaz, S. Foaleng-Mafang, K.-Y. Song, S. Chin, J.-C. Beugnot, N. Primerov, and M. Tur, "Recent progress towards centimetric spatial resolution in distributed fibre sensing," in *(EWOFS'10) Fourth European Workshop on Optical Fibre Sensors*(International Society for Optics and Photonics2010), pp. 765309-765309-765307.
4. G. M. Prisco, "Fiber optic shape sensing," (Google Patents, 2012).
5. M. Froggatt, and J. Moore, "High-spatial-resolution distributed strain measurement in optical fiber with Rayleigh scatter," Applied Optics **37**, 1735-1740 (1998).
6. Y. Wang, J. Gong, B. Dong, D. Y. Wang, T. J. Shillig, and A. Wang, "A Large Serial Time-Division Multiplexed Fiber Bragg Grating Sensor Network," Lightwave Technology, Journal of **30**, 2751-2756 (2012).
7. K. Hotate, and K. Kajiwara, "Proposal and experimental verification of Bragg wavelength distribution measurement within a long-length FBG by synthesis of optical coherence function," Optics Express **16**, 7881-7887 (2008).
8. D. Johnson, "Novel Optical Fibers-Draw-tower process creates high-quality FBG arrays," Laser Focus World **48**, 53 (2012).
9. F. Shen, W. Peng, K. L. Cooper, G. Pickrell, and A. Wang, "UV-induced intrinsic Fabry-Perot interferometric fiber sensors," in *Optics East*(International Society for Optics and Photonics2004), pp. 47-56.
10. L. Yuan, J. Huang, X. Lan, H. Wang, L. Jiang, and H. Xiao, "All-in-fiber optofluidic sensor fabricated by femtosecond laser assisted chemical etching," Optics Letters **39**, 2358-2361 (2014).
11. Y. Zhang, L. Yuan, X. Lan, A. Kaur, J. Huang, and H. Xiao, "High-temperature fiber-optic Fabry–Perot interferometric pressure sensor fabricated by femtosecond laser," Optics Letters **38**, 4609-4612 (2013).
12. W. Wang, D. Ding, N. Chen, F. Pang, and T. Wang, "Quasi-Distributed IFPI Sensing System Demultiplexed With FFT-Based Wavelength Tracking Method," Sensors Journal, IEEE **12**, 2875-2880 (2012).
13. J. Huang, X. Lan, M. Luo, and H. Xiao, "Spatially continuous distributed fiber optic sensing using optical carrier based microwave interferometry," Optics Express **22**, 18757-18769 (2014).